

Interpretation of Water Chemistry and Stable Isotope Data from a Karst Aquifer According to Flow Regimes Identified through Hydrograph Recession Analysis

By D. H. Doctor¹ and E. C. Alexander, Jr.²

¹ U.S. Geological Survey, 345 Middlefield Rd., MS 434, Menlo Park, CA, 94025

² Univ. of Minnesota, Dept. of Geology and Geophysics, 310 Pillsbury Dr. SE, Minneapolis, MN, 55414

ABSTRACT

In this study the relation between flow regime and chemistry of a major karst groundwater resurgence zone in southwestern Slovenia was examined using spring hydrograph recession analysis. Long-term (>2 weeks) recession periods were isolated from 6 years of flow data. Breaks in slope on a plot of the natural log of the discharge versus time allowed for the identification of four separate flow regimes of the aquifer outflow. Major ion chemistry and stable isotopic composition ($\delta^{18}\text{O}$ of water and $\delta^{13}\text{C}$ of DIC) of samples collected twice monthly for two years were then grouped according to where they had been collected within each identified flow regime. Patterns in the chemical and isotopic data emerged which indicated shifting sources of water contributing to the outflow of the spring under different hydrologic conditions. This type of analysis may be a valuable water resource management tool in other karst regions.

INTRODUCTION

A primary challenge for the management of karst water resources is to characterize water quality changes with discharge variability. In order to accomplish this goal, managers must be able to efficiently assess two aspects of the karst aquifer system that interact and determine overall water quality: the hydrologic and the hydrochemical variability. Often, however, resources for characterizing water quality across the full range of hydrologic variability are limited, resulting in a frequency of water sampling that is far lower than the actual time scale of chemical changes taking place at the point of measurement. Therefore, a need exists for a method through which relatively infrequent water quality data can be used to accurately understand and possibly predict major changes in water quality as the hydrologic conditions change.

In this paper, we describe a technique in which long-term records of discharge and relatively infrequent water quality sampling can be combined for the purpose of studying water quality changes with flow. The steps are not mathematically complex, allowing for straightforward and rapid culling of information from data which already exists for many springs. The analysis begins with examination of the recession limbs of a long-term (several years) record

of discharge. First suggested by Maillet (1905), several authors have since proposed that the recession limb of a karst spring hydrograph can be approximated by a function that is the sum of several exponential segments of the total recession (Forkasiewicz and Paloc, 1967; Hall, 1968, Milanović, 1981; Bonacci, 1993; Tallaksen, 1995). Thus, the entire discharge-time relationship of the recession is expressed as:

$$Q(t) = \sum_{i=1}^N q_0^i e^{-(\alpha_i)t} \quad (\text{eq. 1})$$

Where Q is the discharge at time t , N is the number of exponential segments of the recession, q_0^i is the discharge at the beginning of each recession segment, and α_i is the recession coefficient for each segment. In this model, each exponential segment is interpreted to represent the depletion of an aquifer reservoir, with the rate of depletion of that reservoir being represented by the recession coefficient (α_i). Accordingly, the segment with the greatest recession coefficient would represent the most rapid drainage of the karst network (presumably surface runoff or displacement of water into the largest conduits) and the recession segment with the smallest coefficient would represent the baseflow (i.e., the slow drainage of that portion of the aquifer with the lowest transmissivity). The latter is often termed the *diffuse flow*

portion of the aquifer, while the most transmissive conduits are referred to as the *quickflow* portion of the aquifer. Intermediate segments of the total hydrograph recession are thought to represent the emptying of aquifer volumes having intermediate values of hydraulic conductivity.

In reality, it is not clear whether the above conceptual interpretation has any definitive physical validity. It is extremely difficult to quantify the proportions of various transmissive elements of a karst aquifer given the high degree of heterogeneity in karst. Moreover, the conceptual model of a karst aquifer having separate “diffuse flow” and “quick-flow” components may be misleading, as the physical connectivity between fractures and solutionally enlarged conduits exists more as a continuum of transmissivities within the aquifer. Nonetheless, the full recession of the hydrograph contains much useful information, particularly concerning (1) the volume of water drained from the system over time after peak flows, regardless of where the flow originates in the body of the aquifer, and (2) changes in the rate of discharge that occur at discrete values of discharge, thus placing quantifiable limits on aquifer flow regimes.

Constructing a Master Recession Curve

Assuming individual recession segments can be identified, the mean values of q_0 and α for each segment can be used to construct a Master Recession Curve (MRC) of the spring or well (in the absence of identifiable linear segments on a semi-log plot of discharge vs. time, other models may be applied to estimate the segments of the MRC; see Sujono and others, 2004 for examples). Each segment of the MRC is only a portion of an individual exponential recession curve, the constants of which are defined by the values of the recession constant (α) and the initial discharge defining the upper limit of the recession segment (q_0). Taken individually, each of these curves represents aquifer drainage under a particular flow regime, defined by the discharge measured over a specified time interval after the onset of the recession. Except for the tail end of the baseflow recession curve, the time intervals of all of the recession segments overlap. Thus, the volumes of water contributed by the underlying curves must be

accounted for as part of the volume of water drained solely by an individual segment.

For example, let us assume an arbitrary master recession curve of a karst spring, represented in semi-log space in **Figure 1**. Three exponential recession curves ($Q_f(t)$ =fast flow, $Q_i(t)$ =intermediate flow and $Q_b(t)$ =baseflow) combine to give the overall recession, which is represented by the uppermost surface of the intersecting lines shown in Figure 1. The total volume of water drained across the fast flow portion of the recession is equivalent to the integration of recession curve $Q_f(t)$ on the interval t_0 to t_i . In this way, the calculation sums together the volumes V_f^f , V_i^f and V_b^f . Lacking any *a priori* knowledge of the physical significance of these volumes for the functioning of the aquifer, their estimation may not seem consequential. However, for the purposes of water quality interpretation it may be desirable to separate the fastest flow portion from the other volumes drained across the MRC. Thus, we may calculate the fast flow volume (V_F) determined solely by the largest recession constant (α_f) and separated from the baseflow and intermediate flow volumes as:

$$V_F = V_f^f = \int_{t_0}^{t_i} Q_0 \exp(-\alpha_f t) dt - \int_{t_0}^{t_i} q_0^i \exp(-\alpha_i t) dt \text{ (eq. 2)}$$

By integrating the MRC only on the interval from the time of peak flow until the break in slope and intersection with the next recession curve, the expression in eq. 2 quantifies the volume drained solely under the fastest draining portion of the MRC; it is only the volume of the fast flow regime that we seek to define. The “fast flow” volume is not equivalent to the total theoretical volume drained by the uppermost recession curve—rather, it is a flow regime we are defining independent of (but dominated by) that recession curve. The fast flow regime thus includes theoretical contributions from all 3 recession segments.

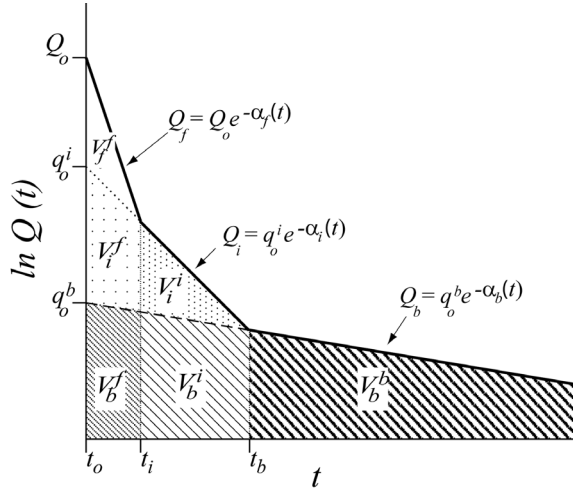


Figure 1. Schematic representation of a Master Recession Curve (MRC) and the theoretical drainage volumes obtained by integration beneath individual linear segments (see text for details).

portion of the MRC; it is only the volume of the fast flow regime that we seek to define. The “fast flow” volume is not equivalent to the total theoretical volume drained by the uppermost recession curve—rather, it is a flow regime we are defining independent of (but dominated by) that recession curve. The fast flow regime thus includes theoretical contributions from all 3 recession segments.

Similarly, the intermediate flow (V_I) and base-flow (V_B) volumes (represented in Figure 1 by the stippled region and cross-hatched region, respectively) can be calculated by the following equations:

$$V_I = \int_{t_0}^{t_b} q_0^i \exp(-\alpha_i t) dt - \int_{t_0}^{t_b} q_0^b \exp(-\alpha_b t) dt \quad (\text{eq. 4})$$

$$V_B = \int_{t_0}^{\infty} q_0^b \exp(-\alpha_b t) dt \quad (\text{eq. 5})$$

Thus, the total volume of water, V_T drained across the entire recession, from $t=0$ to $t=\infty$ is:

$$V_T = V_F + V_I + V_B. \quad (\text{eq. 6})$$

Using these expressions to quantify theoretical volumes of outflow for a particular spring, one may

now look to characterize the quality of water drained from those volumes based upon chemical and/or isotopic data. This was the approach taken for the case study described herein.

STUDY SITE AND BACKGROUND

This study was conducted within the Classical Karst, located along the border between southwestern Slovenia and northeastern Italy. The Slovene name for this region is *Kras*, and this term will be used hereafter in order to signify the geographic location. The *Kras* region is an uplifted, overturned anticlinal block of Cretaceous limestone forming a plateau at approximately 400 m above sea level. The *Kras* region is 40 km long, up to 13 km wide, and covers approximately 440 km², with mean annual precipitation between 1400 and 1600 mm (Kranjc, 1997). Rainfall easily infiltrates into the limestone bedrock, due to thin soil thickness (0 to 0.5 m) and the abundance of bare karst bedrock surfaces. No surface streams exist on the *Kras* plateau. Given the abundant annual precipitation, highly permeable land surface, and lack of surface water runoff, autogenic recharge on the *Kras* surface is a major component of recharge to the underlying aquifer.

In the past, hydrogeological research on the *Kras* focused mainly on the source of water of the Timavo springs. The Timavo springs are the largest natural source of groundwater in the region, and have been an object of curiosity for centuries (Galli, 1999). The largest of these springs has been dived to a depth greater than 80 m below sea level, where phreatic conduits of diameters in the tens of meters have been mapped (Guglia, 1994). Collectively, the long-term average discharge of the springs is approximately 30.2 m³/sec (variable within the years studied between 18 m³/sec and 39.4 m³/sec), with low flows averaging around 9 m³/sec, and maximum flows over 130 m³/sec (Gemiti, 1984).

The Timavo springs represent the major component of outflow (85%) of the regional karst groundwater system (Civita and others, 1995). Several other springs in proximity to the Timavo springs form the remainder of the groundwater resurgence zone. Of these, Sardos spring and Moschenizze North spring are also reclaimed for water supply.

These springs, as well the water from a supply well (B-4) and a monitoring well (B-3) were sampled in this study (**Figure 2**). The water supply well B-4 provides the sole water source for the inhabitants of the Kras region in Slovenia, serving a population of approximately 25,000 people. The monitoring well B-3 is completed within a zone of fluctuating water level, and was observed to be dry after a drought period. Samples collected from the well before and after the drought exhibited nearly identical water chemistry; thus, this well contains water that is displaced from storage within the local vadose zone. A large river, the Soca River, drains the high Julian Alps along the western border between Italy and Slovenia. This river loses a large amount of flow into the karst aquifer ($20 \text{ m}^3/\text{sec}$), and is believed to account for much of the flow from the springs in

affects the outflow of the springs with changing flow conditions.

Daily discharge measurements exist at the Timavo springs as a consequence of their reclamation for water use. In order to quantitatively define the flow regimes considered here, a hydrograph analysis of the Timavo springs discharge was performed. Six years of discharge records were available, from 1995-2000. Out of the six-year record, six of the longest recession periods were chosen for detailed analysis. The recession flows at the Timavo springs were fit by a series of linear segments of the hydrograph recession in semi-log space. The simple exponential decay relation (*eq. 1*) appears to provide an adequate model for the analysis of all discharge regimes at the springs.

METHODS

From our hydrograph recession analysis, a Master Recession Curve (MRC) (**Figure 3**) was constructed. Individual storm event recessions from the long-term discharge records of the Timavo springs were compiled to form the MRC. Four distinct segments to the Timavo MRC were identified, each corresponding to a characteristic flow regime. The breaks in slope define the approximate discharge limits of each flow regime.

The MRC construction was performed manually by visual inspection of the individual event hydrographs. Individual event recession periods were isolated from the entire discharge record and were plotted as the natural log of the flow ($\ln Q$) vs. time (t). **Figure 4** shows one of these recession hydrographs of the Timavo springs. Linear ordinary least-squares regression lines were then fit to each segment of each event hydrograph in semi-log space. The slopes of the regression lines are equal to the values of the recession coefficient (α) for each flow regime of the MRC in units of day^{-1} , and the y-intercept of the regression lines are the value of discharge at the start of the recession (q_0 at $t=0$). The values of α and q_0 that were obtained from the linear regressions of the six event hydrographs were tabulated for each segment of each event, and averaged. These results are presented in **Table 1**.

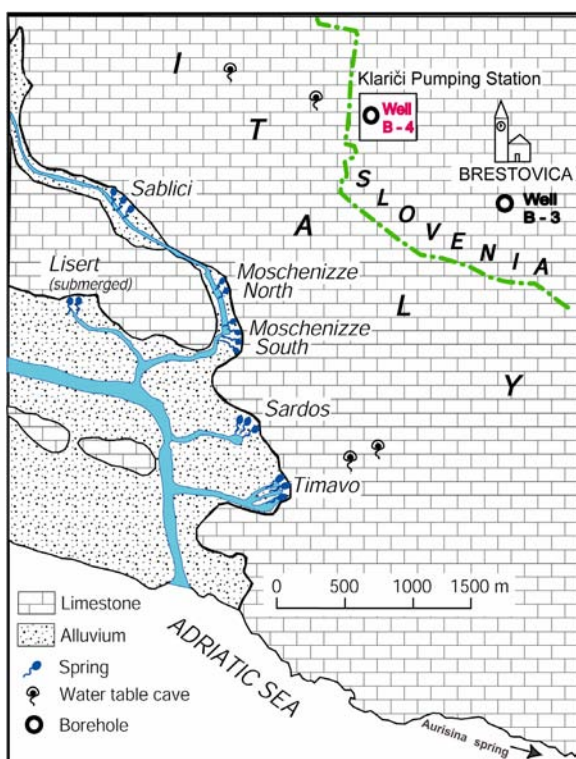


Figure 2. The groundwater resurgence zone of the Kras region (after Krivic, 1981).

the summer (Mosetti & D'Ambrosi, 1963; Urbanc & Kristan, 1998). The primary goal of this study was to determine how the contribution from the Soca River

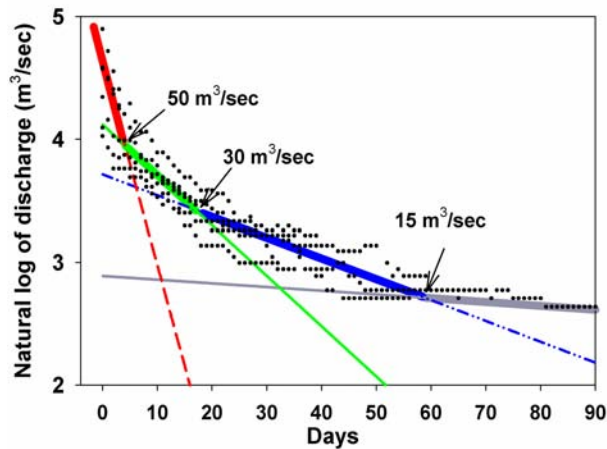


Figure 3. Master Recession Curve for the Timavo springs. Lines indicate ordinary least-squares regression through recession segments. Average daily discharge data are shown as dots.

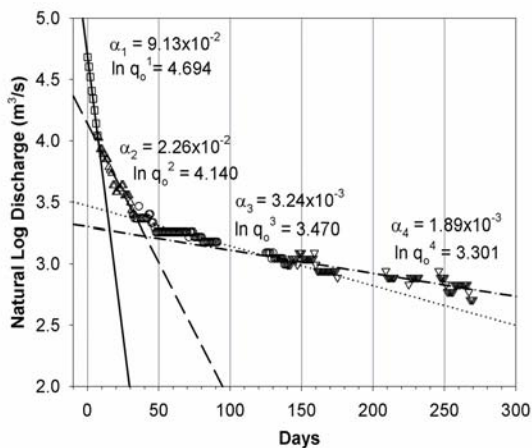


Figure 4. Representative recession hydrograph of the Timavo springs.

Since it was a common occurrence that recession segments would be cut off by increases in discharge resulting from new recharge events, the values of α and q_0 were weighted according to the time duration of each segment prior to an increase in discharge. Thus, values of α and q_0 obtained from individual recessions that persisted for longer time periods were more heavily weighted in the calculation of the mean values for that portion of the MRC. This practice lends a deliberate bias towards the larger events; the largest events recharge a greater

portion of the vadose zone as the water table of the aquifer rises, thus they produce longer, more informative, recessions.

A limitation to the analysis in this case is that the Timavo springs, having been engineered for water reclamation, are fitted with a sluice gate that controls the discharge at low flow. The consequence of the control structures is that the baseflow never drops below $9 \text{ m}^3/\text{sec}$. Thus, the true baseflow recession slope may be absent. Nonetheless, significantly long periods of recession that were not influenced by the control structures were observed such that reproducible recession segments could be fit to the discharge record.

RESULTS AND DISCUSSION

Four flow regimes of the Kras aquifer were defined through the hydrograph analysis: (1) flood flow, (2) high flow (3) moderate flow, and (4) baseflow. The flood flow regime is for flows of the Timavo springs above approximately $50 \text{ m}^3/\text{sec}$, high flow is between 30 and $50 \text{ m}^3/\text{sec}$, moderate flow is between 15 and $30 \text{ m}^3/\text{sec}$, and baseflow discharge is below $15 \text{ m}^3/\text{sec}$.

The individual segments of the MRC were integrated to provide an area below the curve that represents the total theoretical storage volume of the aquifer that supplies the discharge of the Timavo springs. These results are shown in **Table 1**.

Comparison between flow regimes, isotopes, and chemistry

The isotopic and chemical data collected in this study were grouped into the four flow regimes according to the discharge measured at the Timavo springs on the date the water sample was collected. Oxygen ($\delta^{18}\text{O}$ of water) and carbon ($\delta^{13}\text{C}$ of dissolved inorganic carbon, or $\delta^{13}\text{C}_{\text{DIC}}$) stable isotope data of the Timavo springs collected between November 1998 and November 2000 were grouped together by flow regime, and box plots were constructed.

TABLE 1. Results of Timavo springs hydrograph recession analysis

Recession segment	Flow regime	Discharge range (m ³ /sec)	α (day ⁻¹)	q_0 (m ³ /s)	Recession Period (days)	Storage volume (m ³)	% of total storage
1	Flood flow	> 50	1.64×10^{-1}	101.49	0 (peak Q) – 4	0.06×10^8	1.0%
2	High flow	30 to 50	4.10×10^{-2}	61.56	4 – 17	0.13×10^8	2.2%
3	Moderate flow	15 to 30	1.70×10^{-2}	40.98	17 – 58	0.48×10^8	8.2%
4	Baseflow	<15	3.00×10^{-3}	18.00	58 or more	5.18×10^8	88.5%
Total:						5.85×10^8	100 %

The relation between $\delta^{18}\text{O}$ and flow regime is opposite to the relation between $\delta^{13}\text{C}_{\text{DIC}}$ and flow regime (**Figure 5a & 5b**). The $\delta^{18}\text{O}$ values become more negative with higher flow while $\delta^{13}\text{C}_{\text{DIC}}$ values become more positive. The increase in $\delta^{18}\text{O}$ and corresponding decrease in $\delta^{13}\text{C}_{\text{DIC}}$ with increasing flow is consistent throughout the sampling period. In addition, similar seasonal trends are apparent among the isotopic variation of all of the groundwaters (**Figure 6**). Note that all the groundwaters can be approximated as a mixture between the water of well B-3 (autogenic recharge) and the Soca River.

The high-altitude (>2000 m) alpine source of the Soca River lends it $\delta^{18}\text{O}$ values that are more negative than the water derived from local rainfall on the Kras. The $\delta^{18}\text{O}$ of weighted mean annual precipitation is -6.5‰, essentially equal to the composition of well B-3. Thus, the difference in $\delta^{18}\text{O}$ between these sources of water allows for discrimination between them in the mixtures of the groundwaters.

Similarly, the difference in $\delta^{13}\text{C}_{\text{DIC}}$ values between the Soca River and autogenic recharge (represented by the composition of well B-3) adds a second parameter by which to discriminate between these sources in the outflow. Lower $\delta^{13}\text{C}_{\text{DIC}}$ values in the autogenic recharge water reflect a greater proportion of DIC derived from soil CO_2 , which tends to be low in $\delta^{13}\text{C}_{\text{DIC}}$ as a result of the oxidation of organic matter (Deines, 1980; Deines and others, 1974). The partial pressure of CO_2 in the unsaturated zone is 10-100 times that of the atmosphere with $\delta^{13}\text{C}$ values between -20 and -25‰ (Doctor, 2002), thus lower $\delta^{13}\text{C}_{\text{DIC}}$ values indicate water that has been stored within the vadose zone of the karst.

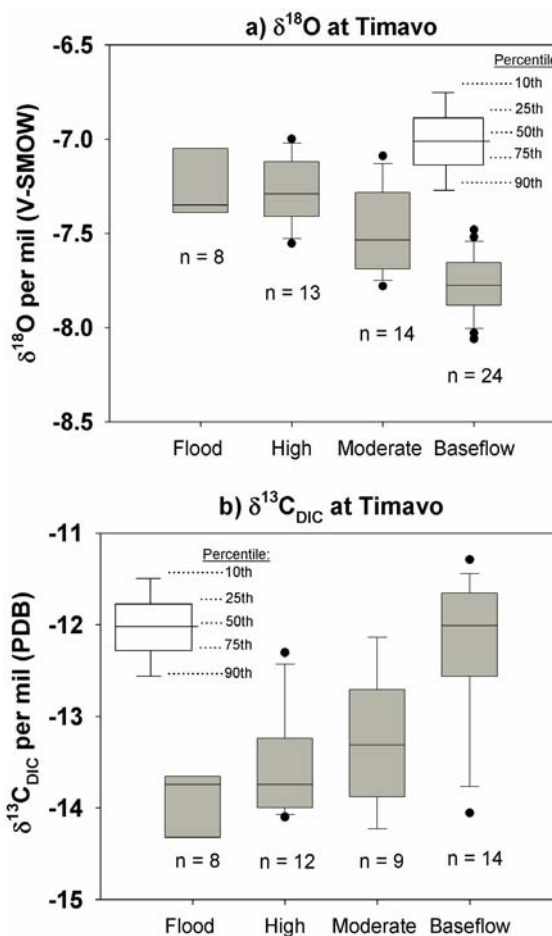


Figure 5. Changes in stable isotopic composition with flow regimes at the Timavo springs. Outlier values correspond to samples collected immediately after or during storm events.

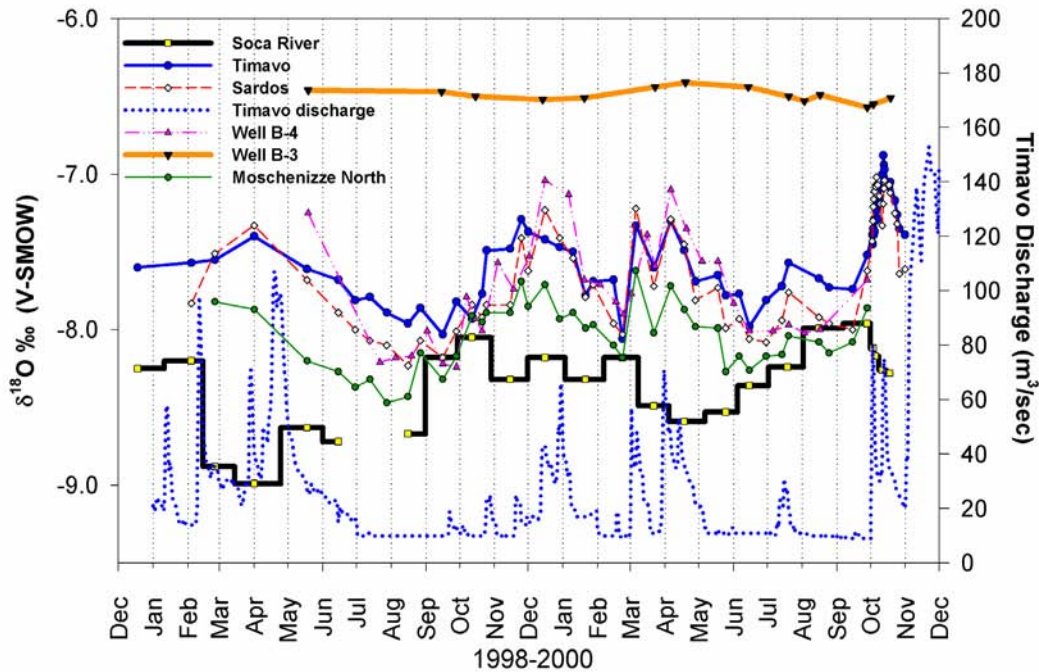


Figure 6. Time series of oxygen isotope values of the Kras groundwaters, with the average daily discharge of the Timavo springs shown for reference. Note that all the groundwaters are a mixture between the water of well B-3 (autogenic recharge) and the Soca River.

Together, these isotopic data present a conceptual model of two component mixing between allogenic Soca River water and autogenic recharge from local precipitation to account for the observed isotopic compositions of the Kras groundwaters. The proportion of Soca River water issuing from the springs is apparently greatest under lower flow conditions, while increasing amounts of autogenic recharge water are released from storage in the vadose zone during higher flows.

The chemistry data from the present study was combined with the chemistry data of Gemiti & Licciardello (1977) and of Cancian (1987), assuming similarity between the flow regimes determined by those authors and the flow regimes determined by the recession analysis of the present study. For the combined chemistry data it was possible to characterize only three flow regimes, since Cancian (1987) reports only three in his data summary. Therefore, the mean values of the flood flow and high flow regime from the recession analysis were combined

into “high flow”, and the baseflow values are defined as “low flow”.

The results of the water chemistries grouped according to flow regime are shown in **Figures 7 to 9**. **Figure 7** shows the Ca/Mg ratios of all the groundwaters tend to approach that of the Soca River as the flow decreases with the exception of well B-4, which shows a relatively constant Ca/Mg ratio regardless of flow regime. Of the other springs, Timavo has the highest Ca/Mg values, followed by Sardos and then by Moschenizze North. Well B-3 has a much higher and constant Ca/Mg than the other waters, thus the progressive shift toward higher Ca/Mg values with increasing flow regime implies a shift toward a greater proportion of autogenic recharge water supplying the springs.

For Cl^- , all of the groundwaters show similar concentrations except for well B-4, which has the highest Cl^- concentrations of all of the groundwaters (**Figure 8**). Cl^- levels in the other groundwaters are relatively constant at 5-10 ppm across the flow

regimes, while for well B-4 the Cl^- is highest at high flow (>50 ppm on average) and decreases to approximately 20 ppm on average at low flow. Well B-3 has a low and constant Cl^- concentration of 3.0 ppm.

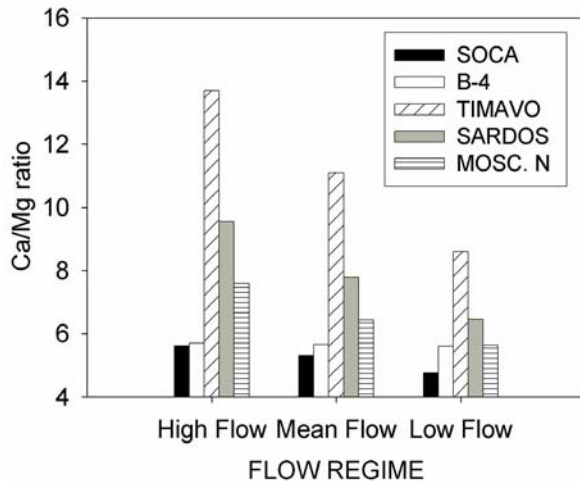


Figure 7. Ca/Mg ratio of Kras groundwaters with flow regime.

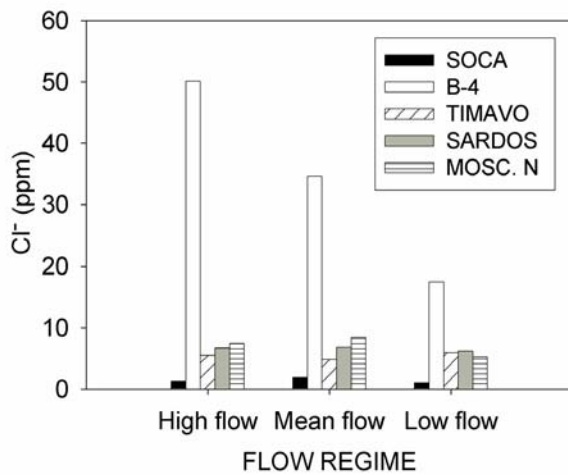


Figure 8. Cl^- of Kras groundwaters with flow regime.

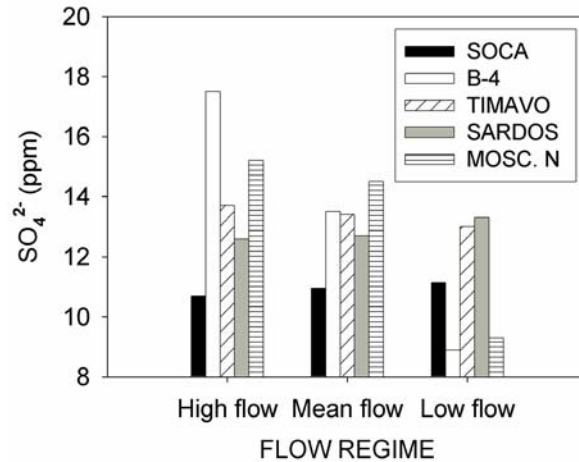


Figure 9. SO_4^{2-} of Kras groundwaters with flow regime.

Well B-4 also shows anomalous chemistry with respect to SO_4^{2-} ; it has the highest SO_4^{2-} concentrations of all the groundwaters at high flow and the lowest SO_4^{2-} at low flow (**Figure 9**). SO_4^{2-} concentrations at Timavo and Sardos stay relatively constant regardless of flow regime, at between 12-14 ppm on average. SO_4^{2-} at well B-4 and Moschenizze North decreases with decreasing flow regime, and at low flow they exhibit the lowest SO_4^{2-} concentrations of all the groundwaters.

High chloride (>100 ppm) and sulfate (>30 ppm) concentrations have been observed from two shafts intersecting the water table nearby the Timavo springs (Gemiti, 1994). The water in these shafts is derived from local storage of autogenic recharge within the epikarst, and may be influenced by anthropogenic activities. This water stored within the unsaturated zone impacts well B-4 and Moschenizze North spring under elevated hydraulic head conditions, and to a lesser extent at low flow. Because these two sites exhibit higher Cl^- and SO_4^{2-} when the water table rises, it is likely that an overflow connection permits the higher salinity water to affect both well B-4 and, to a lesser degree, Moschenizze North spring under high flow conditions.

CONCLUSIONS

Hydrochemical and isotopic data collected at a frequency of approximately twice monthly over a two-year period was interpreted through identification of discrete flow regimes of the karst aquifer by means of hydrograph recession analysis. Grouping the chemistry data together within the defined flow regimes illuminated broad patterns of water quality variability according to changing discharge conditions.

The simple exponential decay model used for fitting multiple linear recession segments to the outflow of the Timavo springs was adequate for determining the flow regimes of the groundwater resurgence of the Slovene Kras region. As a result of the recession analysis, four distinct flow regimes of the Timavo springs have been defined: flood flow ($>50 \text{ m}^3/\text{s}$), high flow ($30\text{--}50 \text{ m}^3/\text{s}$), moderate flow ($15\text{--}30 \text{ m}^3/\text{s}$), and baseflow ($<15 \text{ m}^3/\text{s}$). The estimated storage volume of the baseflow regime represents the greatest proportion (88.5%) of the total theoretical storage volume, with the flood and high flow regimes together representing 3.2%. These percentages highlight the importance of the baseflow regime for providing the majority of flow at the Timavo springs. Although high flows do not drain those portions of the aquifer with a large capacity for water storage, floods are responsible for recharging other parts of the aquifer system, thus flood waters may remain in storage for longer periods of time than otherwise may be indicated by the rapid drainage under higher flow regimes.

The flow at the Timavo springs serves as an adequate proxy for the flow of the other local springs that drain the aquifer. Similar trends in the stable isotopic composition ($\delta^{18}\text{O}$ and $\delta^{13}\text{C}_{\text{DIC}}$) of the water exist among the Timavo springs, Sardos spring, and well B-4 when compared to the discharge of the Timavo springs. For each of these groundwaters, the $\delta^{18}\text{O}$ values are lowest during lowest flow periods and highest during the highest flow periods, while the $\delta^{13}\text{C}_{\text{DIC}}$ values are lowest during high flow and highest during low flow. These results indicate mixing between similar sources at each of these outflow points, as well as a change in the proportions of each source under changing

hydrologic conditions. The more negative $\delta^{18}\text{O}$ and more positive $\delta^{13}\text{C}_{\text{DIC}}$ values of the waters are consistent with a predominant Soca River source during low flow periods, while the more positive $\delta^{18}\text{O}$ and more negative $\delta^{13}\text{C}_{\text{DIC}}$ values are consistent with a predominant source of storage within the vadose zone.

The relations among the flow regimes and water chemistry are similar to the results previously reported by Gemiti and Licciardello (1977) and Cancian (1987). There is a general trend of decreasing Ca/Mg ratio with decreasing flow regime in all of the groundwaters sampled, except for well B-4. Since the Soca River shows the lowest Ca/Mg ratio of all the waters, and autogenic recharge water (well B-3) shows the highest Ca/Mg ratio, the decreasing trend supports the conclusion of variable mixing between the Soca River and autogenic recharge such that under lower flow conditions Soca River water has a greater influence on the groundwater of the aquifer.

The anomalous Cl^- and SO_4^{2-} chemistry observed at the Klarici supply well (well B-4) indicates a high salinity component that affects this well when phreatic head levels are elevated during high flows. Water chemistries of local vadose shafts indicate that the source of this high salinity water is likely a shallow perched zone of water in storage within the epikarst. This water may be anthropogenically impacted.

The trends observed in both isotopic and chemical composition of the groundwaters as flow regimes change indicate that pronounced shifts in the water sources feeding the groundwaters of the Kras aquifer resurgence zone occur as hydrologic conditions vary. These data show that under low flow conditions the outflow contains a greater proportion of Soca River water, while under high flow conditions more water discharged from the springs is derived from the vadose zone. In addition, a third source of water with high levels of Cl^- and SO_4^{2-} exists in vadose storage and influences some of the groundwaters under elevated flow conditions. The techniques developed in this study may be applied to other karst aquifers where water quality and flow monitoring is taking place.

ACKNOWLEDGMENTS

Funding for this work was provided by the United States Fulbright and David L. Boren international fellowship programs. We gratefully acknowledge A.C.E.G.A. Trieste, Italy and Kraški Vodovod, Slovenia for access to sampling sites. Additional samples were provided by Geokarst Engineering s.r.l., Trieste. The first author was kindly hosted by the Dept. of Environmental Sciences at the Jožef Stefan Research Institute, Ljubljana, Slovenia and the GSF Institute for Hydrology, Neuherberg, Germany during this study. Thoughtful reviews by Paul Hsieh and John Tinsley of the U.S. Geological Survey significantly improved this manuscript.

REFERENCES

- Bonacci, O. (1993) Karst springs hydrographs as indicators of karst aquifers. *Hydrological Sciences- Journal des Sciences Hydrologiques*, 38 (1,2), 51-62.
- Cancian, G. (1987) L'idrologia del Carso goriziano-triestino tra l'Isonzo e le risorgive del Timavo. *Studi Trentini di Scienze Naturali*, vol. 64, p. 77-98.
- Civita, M., Cucchi, F., Eusebio, A., Garavoglia, S., Maranzana, F. & Vigna, B. (1995) The Timavo hydrogeologic system: an important reservoir of supplementary water resources to be reclaimed and protected. Proc. Int. Symp. "Man on Karst", Postojna 1993, *Acta Carsologica*, 24: 169-186.
- Deines, P. (1980) The isotopic composition of reduced organic carbon. In: Handbook of Environmental Isotope Geochemistry, Vol. 1 (P. Fritz and J.Ch. Fontes, eds.). Amsterdam: Elsevier, pp. 329-406.
- Deines, P., Langmuir, D., and Harmon, R. (1974) Stable carbon isotope ratios and the existence of a gas phase in the evolution of carbonate ground waters. *Geochimica et Cosmochimica Acta*, vol. 38, p.1147-1164.
- Doctor, D.H. (2002) The Hydrogeology of the Classical Karst (Kras) Aquifer of Southwestern Slovenia. Ph.D. dissertation, University of Minnesota, 252 pp.
- Forkasiewicz, J. and Paloc, H., (1967) Le régime de tarissement de la Foux de la Vis. Etude préliminaire. AIHS Coll. Hydrol. des roches fissurées, Dubrovnik (Yugoslavia), vol. 1, pp. 213-228.
- Galli, Mario (1999) Timavo: Esplorazione e studi. Supplemento no. 23 di *Atti e Memorie della Commissione Grotte "Eugenio Boegan"*, Trieste, 195 pp.
- Gemiti, F. (1984) La portata del Timavo alle risorgive di S. Giovanni di Duino. *Annali Gruppo Grotte Ass. 30° Ott., Trieste*, 7:23-41.
- Gemiti, F. (1994) Indagini idrochimiche alle risorgive del Timavo. *Atti e Memorie della Commissione Grotte "E. Boegan"*, vol. 30, pp 73-83.
- Gemiti, F., and Licciardello, M. (1977) Indagini sui rapporti di alimentazione delle acque del Carso triestino e goriziano mediante l'utilizzo di alcuni traccianti naturali. *Annali Gruppo Grotte Ass. XXX Ott., sez. C.A.I. Trieste*, 6, 43-61.
- Guglia, P. (1994) Risultati esplorativi del Progetto Timavo (1990-1993). *Atti e Memorie della Commissione Grotta "E. Boegan"*, 31/1992-93: 25-48.
- Hall, F.R. (1968) Base-flow recessions—a review. *Water Resources Research*, vol. 4 (5): 973-983.
- Kranjc, A., ed., (1997) Slovene Classical Karst—"Kras". Postojna: Institut za raziskovanja krasa ZRC SAZU, 254 pp.
- Krivic, P. (1981) Etude hydrodynamique d'un aquifère karstique côtière: le Kras de Slovenie, Yougoslavie. Accadèmie Montpellier, Univ. Sc. Techn. Languedoc, Thèse de Docteur-Ingénieur Université Montpellier II: 108 pp.
- Maillet, E. (1905) *Essai d'Hydraulique Souterraine et Fluviale*. Librairie Scientifique A. Hermann: Paris.
- Milanović, P. T. (1981) Karst Hydrogeology. Littleton, Colorado: Water Resources Publications, 434 pp.
- Mosetti, F. & D'Ambrosi, C. (1963) Alcune ricerche preliminari in merito a supposti legami di alimentazione fra il Timavo e l'Isonzo. *Boll. Geograf. Teor. ed Appl.*, n. 17.
- Sujono, J., Shikasho, S., Hiramatsu, K. (2004) A comparison of techniques for hydrograph recession analysis. *Hydrological Processes*, 18, 403-413.

Tallaksen, L.M. (1995) A review of baseflow recession analysis. *Journal of Hydrology*, **165**: 349-370.

Urbanc, J., and Kristan, S. (1998) Isotope investigation of the Brestovica water source during an intensive pumping test. *RMZ - Materials and Geoenvironment*, vol. 45, no. 1-2, p. 187-191.

An Appalachian Regional Karst Map and Progress Towards a New National Karst Map

By D.J. Weary

U.S. Geological Survey, MS926A National Center, Reston, VA 20192

ABSTRACT

A new 1:1 million scale, lithology-based, digital karst map has been constructed for the Appalachian region. This map is serving as the nucleus for a new national karst map and as a test for methodologies used in developing the national karst map and data base. The map comprises data compiled from various state and regional sources. Issues encountered in the compilation process include unevenness between the various data sets in resolution, lithologic description, and classification. Regional geologic and karst data sets providing information on glacial deposits and cave and sinkhole locations are valuable components of the compilation and may also be used as tools for testing the validity of portions of the map and for creating derived products such as karst density maps. Compilation of the national karst map will become more difficult as it progresses to include semi-arid western states that contain evaporate karst, karst aquifers, karstic features propagated from buried evaporites into surface rocks of non-karstic lithology, and various features analogous to karst.

INTRODUCTION

In 2001 the U.S. Geological Survey Karst Applied Research Studies Through geologic mapping (KARST) Project began the task of constructing a new national karst map, which would improve on the Davies and others (1984) 1:7.5 million scale National Atlas karst map. The new map will be digitally-based and constructed, edited and updated in a GIS environment. The working resolution of the new map is 1:1 million scale with paper versions planned at scales of 1:7.5 and 1:2.5 million. As a first step, we are publishing a digital map of karst in the Appalachian states as a U.S. Geological Survey Open-File Report. Production of this map has revealed some of the problems and issues regarding compilation of diverse and inconsistent data sets supplied from various sources.

The Appalachian Region

The Appalachian region, as defined by the Appalachian Regional Commission (ARC) was used as an arbitrary geographic area for our initial compilation effort (fig. 1). This area, based on socioeconomic and political factors, makes a compact swath covering the central and southern Appalachian Mountains, the Piedmont and parts of the eastern Midcontinent, Atlantic Coastal Plain, and the

Gulf Coastal Plain. This area includes the states of New York, Pennsylvania, Ohio, Maryland, Virginia, West Virginia, Kentucky, North Carolina, Tennessee, South Carolina, Georgia, Alabama, and Mississippi. Included on our map, so that it will be complete to the Atlantic coast, are the states of New Jersey and Delaware.

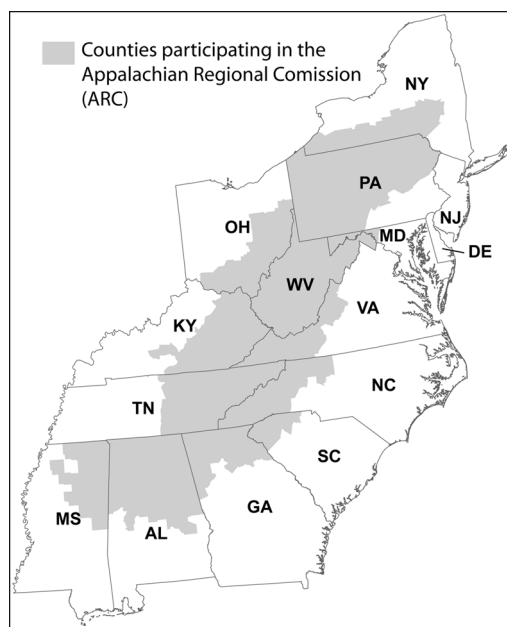


Figure 1. The Appalachian region as defined by the ARC, in gray. States of New Jersey and Delaware are included in this study for completeness to the Atlantic coast.

COMPILATION

Karst and Geologic data

Representatives of all of the state geological surveys in the region were contacted and invited to participate in a workshop on Appalachian karst sponsored by the U.S. Geological Survey and the Kentucky Geological Survey in September, 2002. States that could not attend were asked for sources of karst or geologic data or publicly available geologic data were located on the internet. Karst or geologic data at a scale of 1:1 million or larger were acquired for each state and loaded into ArcMap-ArcInfo for manipulation.

Some states, such as Kentucky and Ohio, already had a state-scale karst map completed (Appendix 1). Those karst areas were simply incorporated into the map and assigned the appropriate attributes. For other areas it is assumed that, in the eastern U.S., where there is sufficient rainfall, carbonate areas, extracted from bedrock maps would suffice as proxies for areas of karst. Geologic units with no carbonates in their unit description were deleted. Lithologic unit descriptions from the original data sets were cross-checked against descriptions in the U.S. Geological Survey National Geologic Map Database (http://ngmdb.usgs.gov/Geolex/geolex_home.html). References to data sources for each state are listed in Appendix 1.

Since the resolution of the individual data sources varied from scales of 1:1 million to 1:24,000 the distance between vertices in the polygon boundaries was generalized in ArcInfo to a spacing of 150 meters for uniformity and to eliminate some of the very small polygons and curves that would not be visible at the working scale of 1:1 million. Also, all polygons with an area of less than 40,000 m² were deleted, as they are too small to portray visibly on the map.

Each polygon was then assigned the following attributes: 1). K_TYPE = an abbreviation for the karst type; state = state name; REF_CODE = reference code, an alphanumeric code to the data source(s).

Structural data

After the areal distribution of potentially karstic rocks was mapped, a scanned and georegistered image of a Tectonic lithofacies map of the Appalachian orogen (Williams, 1978) was used as a visual template for segregating folded and faulted rocks east of the Allegheny structural front from flat-lying to gently dipping rocks to the west. The rationale for this division is the strong influence that the structural nature of the host bedrock has on cave passage patterns and, presumably, other karst features (Palmer, 2000).

Glacial data

Because glacial beveling and cover by glacial sediments has a profound effect on karst distribution in the northern portion of the United States, data on thickness of glacial sediments were integrated into the karst map. Fortunately, a digital dataset of glacial sediment cover for the United States east of the Rocky Mountains already exists (Soller and Packard, 1998). Areas with glacial cover exceeding 50 ft thick (fig. 2) were extracted from this dataset and intersected with the karst areas to define areas of potential karst buried under glacially derived sediments.

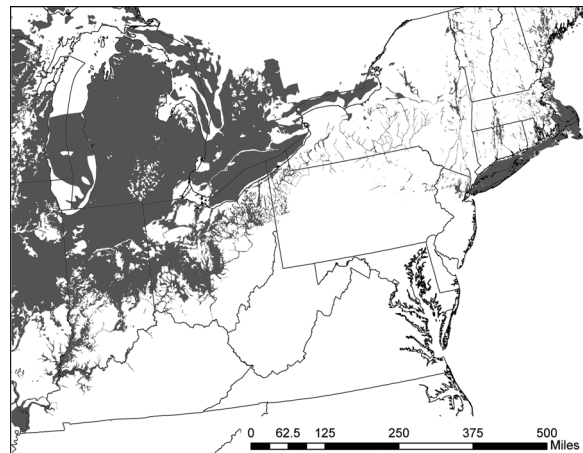


Figure 2. Distribution of glacial sediments greater than 50 ft thick (in gray) in part of the Appalachian region. Derived from data from Soller and Packard (1998).

RESULTS

A draft, first version of the Appalachian karst map is shown in figure 3. A portion of the Davies

and others map (1984) is shown in figure 4 for comparison. The most substantial apparent difference between the two maps is the better resolution of the new map, 1:1 million vs 1:7.5 million. The new map also includes more Atlantic Coastal Plain units as potentially karstic than did Davies and others (1984).

This is the first iteration in a process of compilation and refinement of the map. Publication as a digital product will facilitate release of revised versions as corrections and adjustments are made in the future.

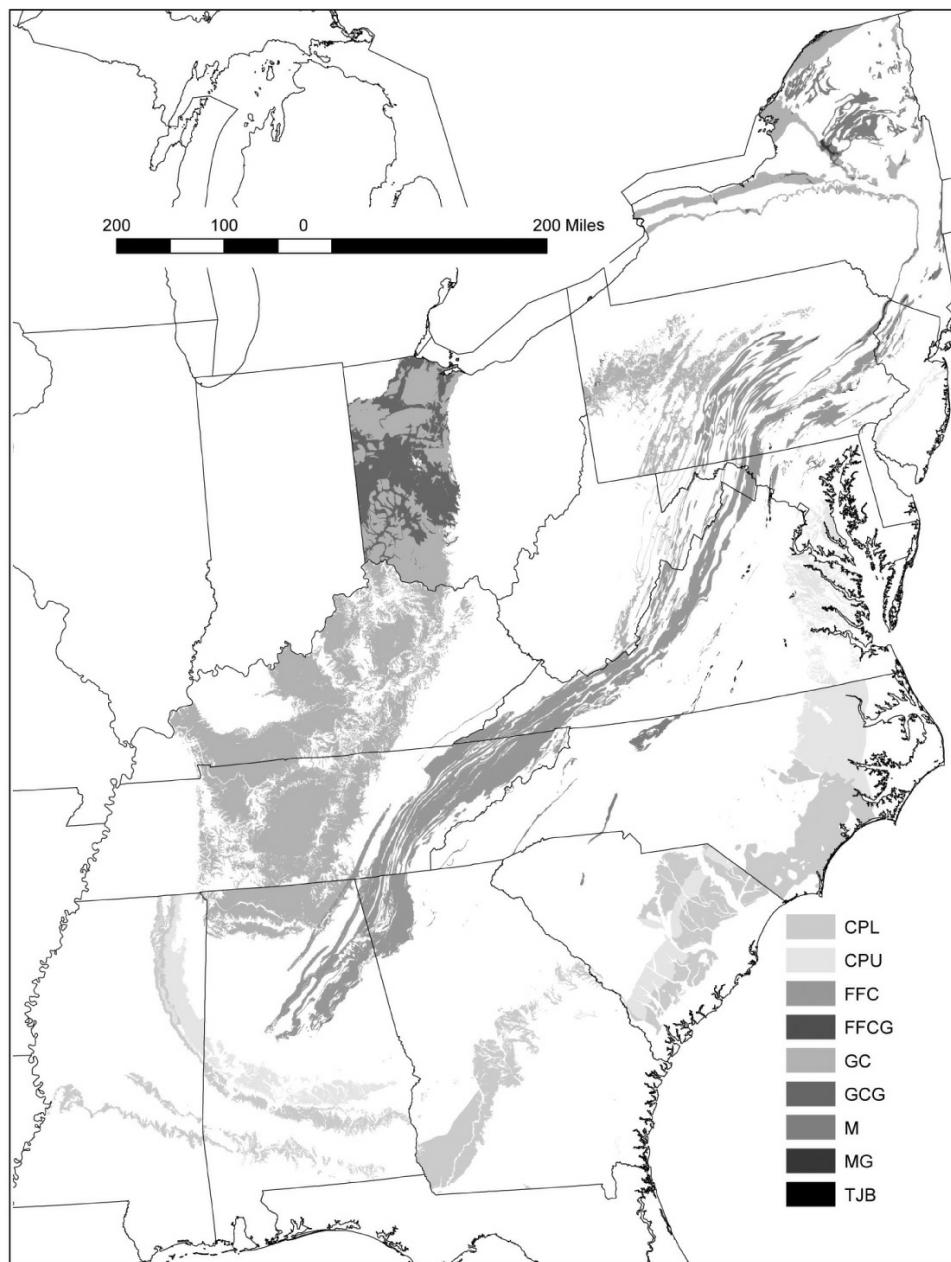


Figure 3. Draft map of Appalachian karst. CPL = Coastal Plain limestones; CPU = Coastal Plain unconsolidated calcareous sediments; FFC = folded and faulted carbonate rocks; FFCG = folded and faulted carbonate rocks with glacial cover greater than 50 ft thick; GC = flat-lying to gently folded carbonate rocks; GCG = flat-lying to gently folded carbonate rocks with glacial cover greater than 50 ft thick; M =marble; MG = marble with glacial cover greater than 50 ft thick; TJB = Triassic and Jurassic basin-fill carbonates.

Description of karst units

Karst-type map units in the new map incorporate lithology, regional structural style, and glacial sedimentary cover greater than 50 ft thick. Further subdivisions and refinements will be made as the project progresses. Full descriptions of the karst-type map units currently assigned follows:

CPU- Coastal Plain unconsolidated: Coastal Plain deposits of unconsolidated, calcareous sediments. Includes chalks, marls, and units with shelly buildups. Dissolution may result in subtle, shallow subsidence sinkholes.

CPL- Coastal Plain limestones: indurated, flat-lying, carbonate rocks. Dissolution may result in solution, collapse, and cover-collapse sinkholes.

FFC- Folded, faulted carbonate rocks: Limestone and dolomite in structurally deformed zones. May be intensely folded and faulted, commonly well jointed, possibly with cleavage. Dissolution may produce solution, collapse, and cover-collapse sinkholes. Caves range from small and simple to long and complex systems. Geometry of cave passage patterns tend to show at least some structural control.

FFCG- Folded, faulted carbonate rocks with glacial cover: Limestone and dolomite in structurally deformed zones covered by 50 ft (15 m) or more of unconsolidated, glacially derived sediment. May be intensely folded and faulted, commonly well jointed, possibly with cleavage. Karst features usually not apparent at surface but solution features probably present at depth.

GC- Gently-folded and flat-lying carbonates rocks: indurated limestone and dolomite that has not been strongly deformed. Predominantly found in interior plateaus and lowlands. Dissolution may produce solution, collapse, and cover-collapse sinkholes. Where carbonates are thick and extensive cave systems may be long and complex. Where thin and interbedded with non-carbonates, caves are small and short. Geometry of cave passage patterns often shows lithologic and bedding-plane control.

GCG- Gently-folded and flat-lying carbonates rocks with glacial cover: indurated limestone and

dolomite that has not been strongly deformed covered by 50 ft (15 m) or more of unconsolidated glacially derived sediment. Predominantly found in interior plateaus and lowlands. Karst features usually not apparent at surface but solution features probably present at depth.

M- Marbles and metalimestones: highly deformed carbonate rocks, usually found in long, thin, linear belts or pods. Dissolution may result in solution, collapse, and cover-collapse sinkholes and small, short caves.

MG- Marbles with glacial cover: highly deformed carbonate rocks, usually found in long, thin, linear belts or pods, covered by 50 ft (15 m) or more of unconsolidated glacially derived sediment. Karst features usually not apparent at surface but solution features probably present at the sediment-rock interface.

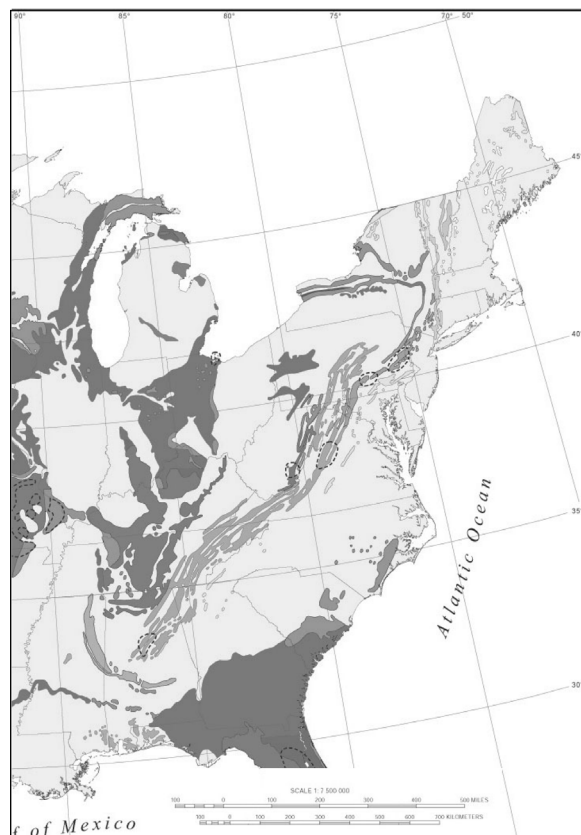


Figure 4. A portion of the digital version of Davies and others (1984) map showing karst areas, in gray tones, in the Appalachian region (Tobin and Weary, 2004).

TJB- Triassic and Jurassic basin fill calcareous sediments. Includes calcareous conglomerates and minor lacustrine limestones. Dissolution may result in solution and subsidence sinkholes and small caves.

DISCUSSION

Problems

Most of the major problems in the new map are differences in delineation of karst areas across state boundaries on state geologic maps. Karst areas for the state of Pennsylvania and the edges of the adjoining states are shown on figure 5 to illustrate some of these differences. Notice that areas delineated as karstic in western Pennsylvania are not currently identified in Ohio and West Virginia. These areas were, however, shown in a gross manner in the Davies and others (1984) (fig. 4) map.

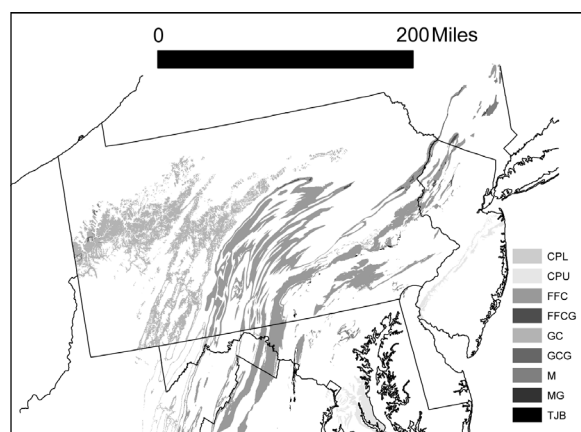


Figure 5. The Pennsylvania portion of the new Appalachian karst map showing discontinuities across boundaries of neighboring states. Explanation of map units as in figure 3.

These areas represent the extent of the Pennsylvanian Allegheny Formation and the Mississippian Mauch Chunk Formation (Miles and others, 2001). The Allegheny Formation comprises chiefly clastic rocks, but also contains the Vanport Limestone which contains caves and other karst features. Likewise, the Mauch Chunk Formation includes the Loyahanna, Greenbrier, Wymps Gap, and Deer Valley Limestones. The Loyahanna and Greenbrier Limestones, in particular, contain caves and other karst features. The Vanport was probably not included in

the state karst map of Ohio (Pavey and others, 2002) because it thins to less than 10 ft thick west of the Ohio River.

Some belts of carbonate units equivalent-in-part to the Mississippian Mauch Chunk Formation continue on into Maryland and West Virginia but are thinner and discontinuous having been subdivided from the thicker clastic units in those states (Peper and others, 2001; West Virginia Bureau of Public Health, 1998).

Ongoing work to compile and refine karst maps of Pennsylvania by Bill Kochanov at the Pennsylvania Geological Survey (oral commun., 2005) will be incorporated in the Appalachian map in the future to revise the extent of karst within that state and will probably resolve most of the boundary mismatches with Maryland and West Virginia. In addition the extent of the Vanport Limestone will probably be extended to the west, feathering-out in eastern Ohio.

A section of the Appalachian karst map centered on the Atlantic Coastal Plain areas of North and South Carolina is shown on Fig. 6. The medium and dark gray areas delineate potentially karstic units derived from individual state data sources. There is not good matching between the mapped Coastal Plain units across the state borders. Differences in lithologic descriptions and each state's classification and grouping scheme affect the aerial extent of the units. Some areas of potential karst, especially in the unconsolidated units, are undoubtedly overstated. Areas of light gray on figure 6 show the extent of potentially karstic units derived from a database for the entire Atlantic Coastal Plain (Newell and others, unpublished data) and areas of very dark gray indicates the overlap of that data set with karst areas delineated by the individual state data. Use of the regional data set eliminates most of the discontinuities between the state boundaries, but, because it is focused on surficial units it does not include some important bedrock limestone units such as the Eocene Castle Hayne Limestone in eastern North Carolina.

Resolution of these problems in the Coastal Plain will require combining the information from the various data sets and a search for more detailed

information on the distribution of calcareous sediments and whether there are, in fact, karst features in some of these units.

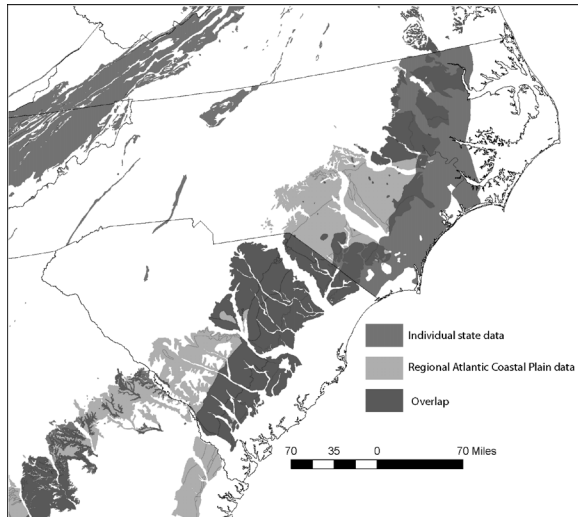


Figure 6. The North and South Carolina part of the new Appalachian karst map showing discontinuities in data sets.

Reported cave locations in the U.S., east of the Mississippi River, plotted on the Appalachian karst map are shown on figure 7. Because they cross state lines and are, presumably, evenly sampled, regional data sets such as this are valuable for checking the accuracy of the karst delineation. Data sets for other karst features, such as sinkhole and spring locations also exist, although most are limited to a particular state or smaller area. If some of these data can be acquired and joined together they will enable further geostatistical analyses of karst across large areas. The density of caves within a part of the Appalachian karst map is shown in figure 8 as an example. This particular plot was generated purely for demonstration purposes, with little thought to rigorous statistical meaning, and should not be taken seriously at this point. It does, however, show interesting patterns in the variation of cave density, with concentrations of caves in central Kentucky, the northeastern corner of Alabama and the southwestern tip of Virginia. Future studies of regional karst feature distribution should lead to new ideas about the effect of tectonism, lithologic facies, hydrologic regime, glaciation, and other factors on the intensity of karstification.

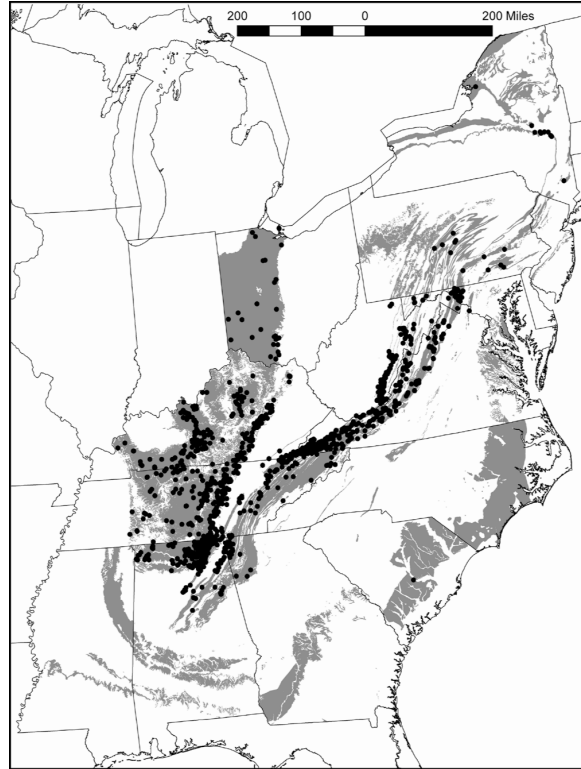


Figure 7. Cave locations (black dots, n=1395) plotted on karst areas in the Appalachians. Cave location data from David Culver, American University, 2004, written communication.

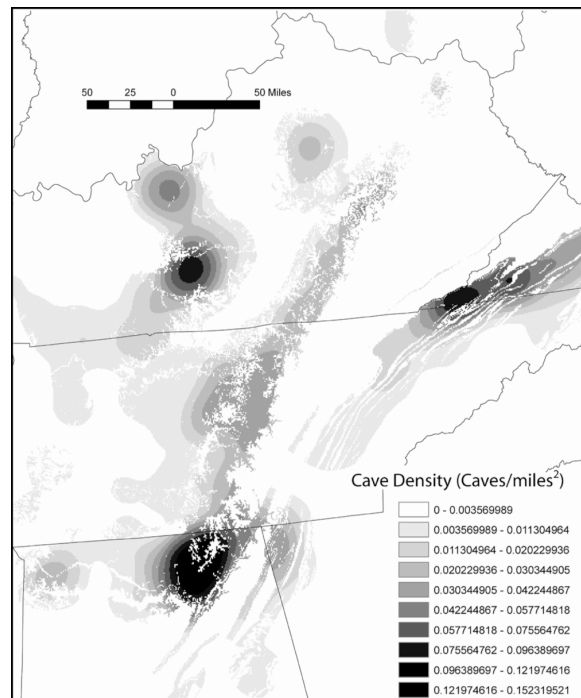


Figure 8. Cave density mapped within the Appalachian karst polygons.

As the nucleus formed by the Appalachian karst map is solidified, state by state coverages, forming the new National Karst map, will be accreted to it. Classifying karst areas in the western part of the country will be a challenge. West of the 32.5-in. mean precipitation line, the nature of weathering and expression of karst features in the United States changes (fig. 9; Epstein and Johnson, 2003). Issues include mapping buried karst, deeply buried evaporates that propagate karst features to non-karstic rocks at the surface, and where to cut the continuum from surface karstic rocks into karst aquifers. A U.S. Geological Survey sponsored workshop involving the state geological surveys of Kansas, Arkansas, Illinois, Iowa, Nebraska, and Wisconsin focusing on these issues will be held August 17 and 18, 2005 at the Kansas Geological Survey. Hopefully we can make some real progress towards generating rules of thumb for mapping these phenomena.

REFERENCES

- Daly, C., and Taylor, G., 2000, United States average annual precipitation, 1961-1990: Spatial Climate Analysis Service, Oregon State University; USDA-NRCS National Cartography and Geospatial Center, Fort Worth, Texas; online linkage: <http://www.ftw.nrcs.usda.gov/prismdata.html>.
- Davies, W.E., Simpson, J.H., Ohlmacher, G.C., Kirk, W.S., and Newton, E.G., 1984, Engineering aspects of karst: U.S. Geological Survey, National Atlas, scale 1:7,5000.
- Dunrud, C.R., and Nevins, B.B., 1981, Solution mining and subsidence in evaporate rocks in the United States: U.S. Geological Survey Miscellaneous Investigation Series Map I-1298, 2 sheets.
- Epstein, J.B., and Johnson, K.S., 2003, The need for a national evaporate karst map, in Johnson, K.S. and Neal, J.T., eds., *Evaporite karst and engineering/environmental problems in the United States*: Norman, Oklahoma Geological Survey, Circular 109, p. 21-30.
- Johnson, K.S., 1997, *Evaporite karst in the United States: Carbonates and Evaporites*, v. 12, p. 2-14.
- Miles, C.E., Whitfield, G.T. and other staff and interns of the Pennsylvania Geological Survey, 2001, *Bedrock geologic units of Pennsylvania*, based on: Berg, T.M., Edmunds, W.E., Geyer, A.R., Glover, A.D., Hoskins,

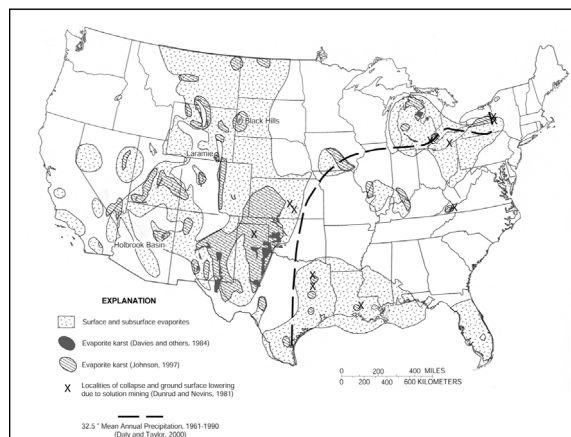


Figure 9. Map showing distribution of outcropping and sub-surface evaporate rocks in the United States and areas of reported evaporate karst. The 32.5-in. mean-annual-precipitation line approximates the boundary between eastern and western karst (from Epstein and Johnson, 2003, fig. 5)

- D.M., MacLachlan, D.B., Root, S.I., Sevon, W.D., and Socolow, A.A., 1980, *Geologic map of Pennsylvania*: Pennsylvania Geological Survey, Map 1, scale 1:250000. <http://www.dcnr.state.pa.us/topogeo/map1/bedmap.aspx>
- Palmer, A.N., 2000, Hydrogeologic control of cave patterns, in Klimchouk, A.B. and others, eds., *Speleogenesis evolution of karst aquifers*: Huntsville, National Speleological Society, p. 77-90.
- Pavey, R.R., Hull, D. N., Brockman, C. S., Schumacher, G. A., Stith, D. A., Swinford, E. M., Sole, T.L., Vorbau, K. E., Kallini, K. D., Evans, E. E., Slucher, E. R., and R. G. Van Horn, 2002, *Known and probably karst in Ohio, 2002*: Ohio Geological Survey, EG-1, version, GIS data on CD provided by the Ohio Geological Survey, scale 1:24,000.
- Peper, J.D., McCartan, L.B., Horton, J.W., Jr., and Reddy, J.E., 2001, Preliminary lithochemical map showing near-surface rock types in the Chesapeake Bay watershed, Virginia and Maryland: U.S. Geological Survey Open-File Report 01-187, resolution 1:500,000. Maryland part based on the Cleaves, 1968, *Geologic map of Maryland*. <http://pubs.usgs.gov/openfile/of01-187/>
- Soller, D.R. & Packard, P.H. (1998). Digital representation of a map showing the thickness and character of Quaternary sediment in the glaciated United States east of the Rocky Mountains: U.S. Geological Survey

Digital Data Series DDS-38, scale 1:1,000,000. <http://pubs.usgs.gov/dds/dds38/shape.html>

Tobin B.D. and Weary, D.J., 2004, Digital Engineering Aspects of Karst Map: A GIS Version of Davies, W.E., Simpson, J.H., Ohlmacher, G.C., Kirk, W.S., and Newton, E.G., 1984, Engineering Aspects of Karst: U.S. Geological Survey, National Atlas of the United States of America, Scale 1:7,500,000. <http://pubs.usgs.gov/of/2004/1352/>

West Virginia Bureau of Public Health, 1998, Karst regions derived from 1968 geological map of West Virginia: West Virginia GIS Technical Center, online data <http://wvgis.wvu.edu/data/dataset.php?action=search&ID=133>, resolution 1:250,000.

Williams, Harold, compiler, 1978, Tectonic lithofacies map of the Appalachian orogen: St John's : Memorial University of Newfoundland, scale 1:1 000,000.

APPENDIX 1

State by state annotated sources for karst and geologic data (in alphabetical order)

Alabama - Szabo, M.W., Osborne, W.E., Copeland, C.W., Jr., and Neathery, T.L., 1988, Geologic Map of Alabama: Geological Survey of Alabama, Special Map 200; digital version: Digital geologic map of Alabama, Beta Version 1, 2002: Geologic Survey of Alabama, scale 1:250,000. [Used for entire state]

Delaware - Nenad Spoljaric, Jordan, R.R., Generalized geologic map of Delaware, revised 1976 by Pickett, T.E.: Delaware Geological Survey, 1 sheet, scale ca. 1:600,000. [Map scanned and digitized at U.S. Geological Survey; Used for entire state]

Georgia - Alhadeff, J.S., Musser, J. W., Sandercock, A.C., and Dyar, T.R., 2001, Digital environmental atlas of Georgia: Georgia Geologic Survey Publication CD-1, ver. 2., scale 1:250,000. [Used for entire state]

Kentucky - Paylor, R.L., and Currens, J.C., 2002, Karst Occurrence in Kentucky: Kentucky Geological Survey, KGS Map and Chart 33, scale 1:500,000. <http://www.uky.edu/KGS/water/general/karst/karst-gis.htm> . [Used for entire state].

Maryland - Peper, J.D., McCartan, L.B., Horton, J.W., Jr., and Reddy, J.E., 2001, Preliminary litho-geochemical map showing near-surface rock types in the Chesapeake Bay watershed, Virginia and Maryland: U.S. Geological Survey Open-File Report 01-187, resolution 1:500,000. Maryland part based on the Cleaves, 1968, Geologic map of Maryland. <http://pubs.usgs.gov/openfile/of01-187/> [Used for entire state, except Coastal Plain]

Newell, W. L, Prowell, D., Kranz, D., Powars, D., Mixon, R., Weems, R., Stone, B., and Willard, D., Surficial geology and geomorphology of the Atlantic Coastal Plain: U.S. Geological Survey, unpublished data.; [Used in Coastal Plain only]

Mississippi - Online data from Mississippi Automated Resource Information System (MARIS) at: http://www.maris.state.ms.us/HTM/Data%20Warehouse/Statewide_alpha.htm. No metadata available (4/2004) scale 1:500,000. [Map units compared with descriptions on published paper maps: 1. Bicker, A.R. Jr., (compiler) 1985, Geologic Map of Mississippi: Mississippi Geological Survey, scale 1:500,000. 2. Booth, D.C. and Schmitz, D.W. (compilers), 1983, Economic minerals map of Mississippi: Mississippi Bureau of Geology, Mississippi Mineral Resources Insititute, scale 1:500,000.]

New Jersey - Vector graphic files of karst units of New Jersey were supplied by Donald Monteverde, New Jersey Geological Survey and were converted to GIS at the U.S. Geological Survey. These units were extracted from: 1.) Dalton, R.F., 1996, Bedrock geologic map of northern New Jersey: U.S. Geological Survey, Miscellaneous Investigations Series, I-2540-A, scale 1:100,000. 2.) Owens, J.P., Sugarman, P.J., Sohl, N.F., Parker, R.A., Houghton, H.F., Volkert, R.A., Drake, A.A., and Orndorff, R.C., 1995, Geologic map of New Jersey: central sheet: New Jersey Geological Survey, scale 1:100,000. 3.) Owens, J.P., Sugarman, P.J., Sohl, N.F., Parker, R.A., Houghton, H.F., Volkert, R.A., Drake, A.A., and Orndorff, R.C., 1995, Geologic map of New Jersey: southern sheet: New Jersey Geological Survey, scale 1:100,000. [Used for entire state.]

New York - Fickies, R.H. and Fallis, E., 1996, Rock Type Map of New York State: New York State Geological Survey, Open file Report 1g1222, scale 1:1,000,000. [GIS data provided by the New York Geological Survey; Used for entire state.]

North Carolina - North Carolina Geological Survey, 1999, Geology - North Carolina: North Carolina Department of Environment and Natural Resources -Division of Land Resources, North Carolina Corporate Geographic Database online data, <http://www.geology.enr.state.nc.us/gis/geol250d.htm>. resolution 1:250,000. [Calcareous rocks extracted based on description of map units. Used for entire state.]

Ohio - Pavey, R.R., Hull, D. N., Brockman, C. S., Schumacher, G. A., Stith, D. A., Swinford, E. M., Sole, T.L., Vorbau, K. E., Kallini, K. D., Evans, E. E., Slucher, E. R., and R. G. Van Horn, 2002, Known and probable karst in Ohio, 2002: Ohio Geological Survey, EG-1, version, GIS data on CD provided by the Ohio Geological Survey, scale 1:24,000. [Polygons generalized and reclassified. Used for entire state.]

Pennsylvania - Miles, C.E., Whitfield, G.T. and other staff and interns of the Pennsylvania Geological Survey, 2001, Bedrock geologic units of Pennsylvania, based on: Berg, T.M., Edmunds, W.E., Geyer, A.R., Glover, A.D., Hoskins, D.M., MacLachlan, D.B., Root, S.I., Sevon, W.D., and Socolow, A.A., 1980, Geologic map of Pennsylvania: Pennsylvania Geological Survey, Map 1, scale 1:250000. <http://www.dcnr.state.pa.us/topogeo/map1/bedmap.aspx> [Carbonate units extracted based on map descriptions. Used for Entire state.]

South Carolina - Horton, J.W. Jr., 2001, Preliminary digital geologic map of the Appalachian Piedmont and Blue Ridge, South Carolina Segment: U.S. Geological Survey, Open-file Report 01-298, <http://pubs.usgs.gov/openfile/of01-298/>, scale 1:500,000. [Carbonate units extracted based on unit labels and descriptions of units found in the U.S. Geological Survey Geologic names lexicon: http://ngmsvr.wr.usgs.gov/Geolex/geolex_home.html; Used for Blue Ridge and Piedmont Provinces only.]

Newell, W. L, Prowell, D., Kranz, D., Powars, D., Mixon, R., Weems, R., Stone, B., and Willard, D., Surficial geology and geomorphology of the Atlantic Coastal Plain: U.S. Geological Survey, unpublished data: [Carbonate units extracted based on unit labels and descriptions of units found in the U.S. Geological Survey Geologic names lexicon: http://ngmsvr.wr.usgs.gov/Geolex/geolex_home.html; Used for Coastal Plain province only.]

Tennessee - Greene, D.C., and Wolfe, W.J., 2000, Superfund GIS – 1:250,000 geology of Tennessee: U.S. Geological Survey, digital version of Tennessee Division of Geology, 1966, Geologic map of Tennessee: Tennessee Division of Geology, William D. Hardeman, State Geologist, 4 sheets, scale 1:250,000. <http://water.usgs.gov/GIS/metadata/usgswrd/geo250k.html> [Calcareous rocks extracted based on description of map units. Used for entire state.]

Virginia - Virginia Division of Mineral Resources, 2003, Digital representation of the 1993 geologic map of Virginia: Virginia Division of Mineral Resources Publication 174 [CD-ROM; 2003, December 31]. Adapted from Virginia Division of Mineral Resources, 1993, Geologic map of Virginia and Expanded Explanation: Virginia Division of Mineral Resources, scale 1:500,000. [Calcareous rocks extracted based on description of map units. Used for entire state.]

West Virginia - West Virginia Bureau of Public Health, 1998, Karst regions derived from 1968 geological map of West Virginia: West Virginia GIS Technical Center, online data <http://wvgis.wvu.edu/data/dataset.php?action=search&ID=133>, resolution 1:250,000. [Used for entire state.]